Check for updates

JGR Planets

RESEARCH ARTICLE
10.1029/2025JE009252

# Geomorphological Evidence of Fluid Seepage in Pit Complex Formation, Pioneer Terra, Pluto

**Roodra Manogaran[1], Gangkai Poh[2,3], Caitlin Ahrens[3,4], Kathleen Mandt[3], and Suniti Karunatillake[1]**

[1]Planetary Science Lab, Department of Geology and Geophysics, Louisiana State University, Baton Rouge, LA, USA, [2]Department of Physics, The Catholic University of America, Washington, DC, USA, [3]NASA Goddard Space Flight Center, Greenbelt, MD, USA, [4]University of Maryland College Park, NASA Goddard Space Flight Center, Greenbelt, MD, USA

**Key Points:**

- Pits in Pioneer Terra exhibit morphological characteristics consistent with seepage-related collapse features on Earth called gas pockmarks
- We proposed that these pits may have formed through fluid migration along extensional faults and seepage driven by subsurface fluids
- This suggests the possible presence of a volatile reservoir with implications for subsurface-surface interactions on icy worlds

**Supporting Information:**

Supporting Information may be found in the online version of this article.

**Correspondence to:**

R. Manogaran,
rmanog1@lsu.edu

**Citation:**

Manogaran, R., Poh, G., Ahrens, C., Mandt, K., & Karunatillake, S. (2026). Geomorphological evidence of fluid seepage in pit complex formation, Pioneer Terra, Pluto. *Journal of Geophysical Research: Planets*, *131*, e2025JE009252. https://doi.org/10.1029/2025JE009252

Received 9 JUN 2025
Accepted 10 FEB 2026

**Author Contributions:**

**Conceptualization:** Roodra Manogaran
**Funding acquisition:** Gangkai Poh
**Investigation:** Roodra Manogaran
**Methodology:** Roodra Manogaran
**Supervision:** Gangkai Poh
**Writing – original draft:** Roodra Manogaran
**Writing – review & editing:** Roodra Manogaran, Gangkai Poh, Caitlin Ahrens, Kathleen Mandt, Suniti Karunatillake

© 2026. American Geophysical Union. All Rights Reserved.

**Abstract** Pluto exhibits widespread pit complexes thought to originate from endogenic processes, possibly involving gaseous effusions from the subsurface, though their formation mechanism remains elusive. Here, we analyze the geomorphology of 150 pits and surrounding features using New Horizons imagery. The pit complex in Pioneer Terra features tectonic lineations and shares distinct morphologies as evidenced by their distribution, cross-sectional, and planform shapes. Drawing parallels with terrestrial analogs, we propose that these pits are potential candidates for fluid migration and seepage events, formed similarly to gas pockmarks in areas with seepage activity on Earth. Our findings imply the presence of volatile reservoirs in Pluto's subsurface, that may episodically release volatiles affecting local landscapes and contributing to the atmosphere. We offer a conceptual model for fluid migration and seepage in the formation of pits in this region, which may also occur across other icy worlds. Future investigations of fluid source and plumbing systems, together with our geomorphic analysis, would further elucidate processes and properties in Pluto's subsurface, thereby advancing our understanding of Pluto's broader geophysical and atmospheric evolution.

**Plain Language Summary** Pluto's surface features pits that may have formed through the release of materials from beneath the surface. Here, we identified and analyzed 150 pits in Pioneer Terra using New Horizons imagery to measure and characterize their morphologies and surrounding features. Based on their characteristics, we propose that the pits share physical similarities with gas pockmarks on Earth formed via fluid migration and seepage. These findings could have important implications for the understanding of material exchange between the subsurface, surface, and atmosphere of icy worlds throughout the solar system.

## 1. Introduction

Pits are geomorphological features observed across planetary bodies in the solar system and are indicators of complex geophysical processes, such as localized cavernous collapse (Rodríguez et al., 2005) and dilational faulting on Mars (Wyrick et al., 2004) and Enceladus (E. S. Martin et al., 2017), diapirism on Europa (Singer, McKinnon & Schenk, 2021), and cryovolcanism on Titan (Lopes et al., 2013). Pluto is no exception, with a widespread occurrence of pits found on the northern and eastern margins of Sputnik Planitia (Howard et al., 2017). In contrast to other regions in the encounter hemisphere, pits observed on faults in East Sputnik are often expressed as pit chains (McGovern et al., 2021). Despite observing pits on many planetary bodies, pit formation and its relation to subsurface interpretation remain poorly understood due to data constraints (Wyrick & Buczkowski, 2022), including that on Pluto. While Howard et al. (2017) previously examined pit morphologies on the north and east of Sputnik Planitia, this study expands on previous work by proposing a terrestrial analogy with fluid seepage observed in oceanic and icy environments, offering a new perspective on their potential links to subsurface processes. Fluid seepage features have been documented in terrestrial and submarine permafrost (Chuvilin et al., 2020) as well as in marine cold seeps (Ceramicola et al., 2018). However, across these settings, the main components of fluid seepage systems are comparable: (a) subsurface fluid source, (b) plumbing system or fluid migration pathways through permeable layers, joints, faults, fractures, or breaches in the overlying lithology, and (c) surface manifestations of fluid seepage (Oehler & Etiope, 2017; Talukder, 2012). These components are central to investigating fluid seepage as a potential mechanism in pit formation on Pluto, and the parallels are explored further in the discussion section.

21699100, 2026, 3, Downloaded from https://agupubs.onlinelibrary.wiley.com/doi/10.1029/2025JE009252 by Nasa Goddard, Wiley Online Library on [02/03/2026]. See the Terms and Conditions (https://onlinelibrary.wiley.com/terms-and-conditions) on Wiley Online Library for rules of use; OA articles are governed by the applicable Creative Commons License

Fluid seepage on Earth commonly exhibits a range of surface manifestations, including gas vents, mounds (e.g., mud volcanoes), and depressions such as gas pockmarks. Mud volcanoes, which can reach heights of ∼200 m, illustrate how subsurface fluids mobilize material kilometers below the surface (Ceramicola et al., 2018). Meanwhile, gas pockmarks typically form through the collapse of surface materials above zones where over pressured fluids migrate upward through subsurface conduits. Such features are reliable geomorphological indicators of localized fluid migration (Ceramicola et al., 2018). The size and distribution of gas pockmarks are contingent upon several contributing factors, including the proximity of a fault system acting as conduits for gas migration, the location and depth of gas sources such as clathrate hydrates, underlying lithology, and subsurface pressure conditions (Hovland et al., 2002). Gas pockmarks typically range from meters across, while mega pockmarks can have diameters exceeding 1 km, with depths from a few meters to more than 200 m (Ceramicola et al., 2018; Wu et al., 2023). Their planform shapes vary from circular and elliptical to elongated or crescentic forms, often reflecting the influence of local slopes, mass wasting, or hydrate decomposition (Andresen et al., 2008; Riboulot et al., 2016; K. Zhang et al., 2023). Pockmarks frequently occur in clusters or form linear chains aligned along faults or weakness zones, which strongly couples their spatial distribution to regional structural controls (Ceramicola et al., 2018; Hovland et al., 2002). Their cross-sectional profiles commonly display U-, V-, W-, or tabular shapes that can represent multiple episodes of fluid expulsion (Andresen et al., 2008). Raised rims may appear where collapse or sediment expulsion accentuates edges (Forwick et al., 2009). Morphometric analysis including diameter, depth, slope, eccentricity, and orientation of pockmarks on Earth has significantly constrained the regional and local geological controls of gas expulsion (Gafeira et al., 2018; Webb et al., 2009). Given that the pit complexes in Pioneer Terra lie below the surrounding terrain (Howard et al., 2017), we investigated whether their formation may be conceptually comparable to terrestrial collapse-related depressions such as pockmarks. Gas pockmarks in both marine sediments and especially permafrost settings therefore provide a conceptual framework for evaluating pit formation in Pluto's volatile-rich, ice-dominated crust, while recognizing that environmental conditions and physical scales differ substantially.

Our region of interest is to the northeast of Sputnik Planitia, in the Hayabusa Group (White et al., 2021), and falls within Pioneer Terra (Figure 1), spanning latitudes 43° to 54°N and longitudes 201° to 216°E. Although the study area overlaps both Pioneer Terra and Hayabusa Terra, its longitudinal extent more closely corresponds to Pioneer Terra (Emran et al., 2023). Pioneer Terra has also been proposed as a favorable site for cryovolcanic activity, potentially facilitated by lithospheric stresses associated with the formation and infilling of Sputnik Planitia (McGovern et al., 2021). Here, we use the term “fluid seepage” to emphasize the specific subsurface-to-surface fluid migration processes, which are widely observed in terrestrial settings and fall under the broader category of cryovolcanism (Howard et al., 2017; C. R. Martin & Binzel, 2021). Notably, while our study area overlaps with a climate zone characterized by permanent tropics, the oscillation range of the arctic circle varies between 13° and 37°, indicating that this region is currently both tropical and arctic (Binzel et al., 2017). The study area located within Pluto's permanent tropical arctic region is interpreted to undergo maximum cyclical extremes (Binzel et al., 2017). Gaseous emissions from larger, deeper pits in northern Pioneer Terra and a declining impact rate may have contributed to the emplacement of thicker mantling deposits and the low density of impact craters in Pioneer and Hayabusa Terrae (Stern et al., 2021).

We specifically investigated the geomorphological characteristics of pit complexes (Figures 1 and 2) within the eroded smooth uplands (Howard et al., 2017). Previous studies have identified a kilometer-scale pit complex within Hayabusa and Pioneer Terrae that appears to be influenced by a local tectonic lineation (Howard et al., 2017; Stern et al., 2018) consistent with surface collapse (Moore et al., 2016; White et al., 2021). Five possible mechanisms have been discussed to form pitted terrains on the uplands north and east of Sputnik Planitia (Howard et al., 2017): (a) surface collapse into subsurface voids due to tensional fractures or removal of ice, (b) differential sublimation of ice (Moore et al., 2017), (c) eruption of subsurface materials, (d) impact cratering, and (e) differential deposition of materials causing relief development around pits (Moore et al., 2016). However, some of these mechanisms have been ruled out based on other geomorphologic observations and association with surrounding geologic structures (Howard et al., 2017). For instance, the extensivity of some pit complexes coupled with the substantial volume of material loss cannot be explained just by tensional fracturing. Pits with elevated rims are associated with structural lineations, most likely ruling out impact cratering. Since pitting is clearly incised below the surrounding terrain in addition to the association between pits and tectonic lineations, constructive or eruptive origin is not the dominant process but likely through the removal of subsurface materials causing surface collapse (Howard et al., 2017). Volatile sublimation is also unlikely to be the dominant

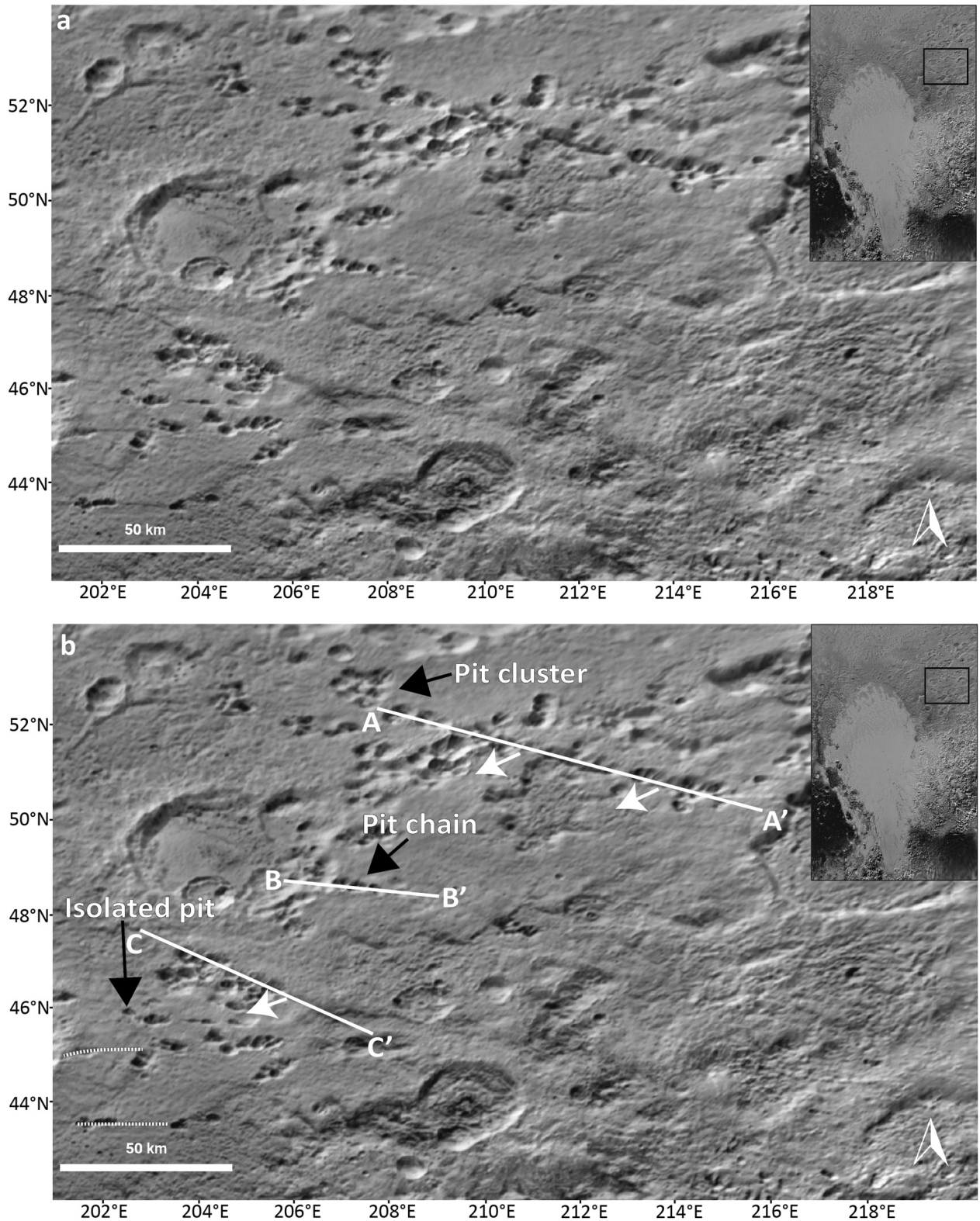


**Figure 1.** (a) Unannotated and (b) annotated global mosaic of the study area showing the studied pit complex and the surrounding features on a cylindrical map projection centered on 180°. The elevation profile paths of faults are shown as A-A′, B-B′, and C-C'. The elevation profiles are displayed in Figure 3. The dashed lines are interpreted as possible faults. Higher pit abundance is located on the southern side of Faults A and C (white arrows). An example of each pit group type, cluster, chain, and isolated, is annotated (black arrows). The inset shows the location of the study area in relation to Sputnik Planitia.



21699100, 2026, 3, Downloaded from https://agupubs.onlinelibrary.wiley.com/doi/10.1029/2025JE009252 by Nasa Goddard, Wiley Online Library on [02/03/2026]. See the Terms and Conditions (https://onlinelibrary.wiley.com/terms-and-conditions) on Wiley Online Library for rules of use; OA articles are governed by the applicable Creative Commons License

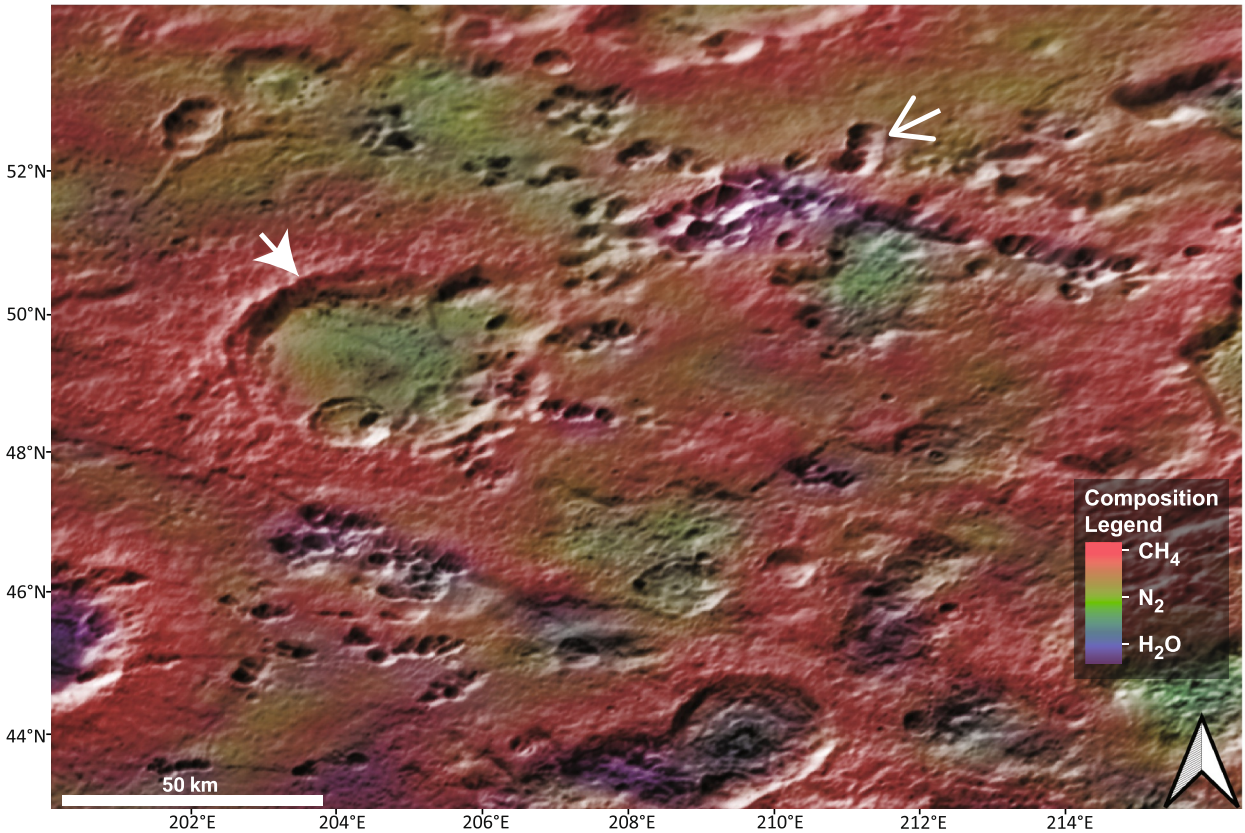


**Figure 2.** Surface composition of the study area based on LEISA imaging spectrometer (Schmitt et al., 2017) overlaid on the global mosaic of Pluto on a cylindrical map projection centered on 180°. Shown are overlaid band depth maps for spectral indicators of $CH_4$ (1.589–1.833 μm), $N_2$ (2.136–2.160 μm), and $H_2O$ (1.39–2.06 μm) using QGIS. Dimensionless band depth values, ranging approximately from −0.05 to 0.55 for $CH_4$, 0.01 to 0.228 for $N_2$, and 0 to 1 for the $H_2O$ spectral indicator. Color bands correspond to relative abundances of $CH_4$-rich ices (red), $N_2$-rich ices (green), and $H_2O$-ices (blue), whereas mixed colors indicate intermediate compositions. Colors in the legend were adapted from Figure 13a of Howard et al. (2017). Two examples of crater-like features are annotated; the arrow with a closed form indicate feature was interpreted as impact crater (excluded from analysis) while arrow with open form was interpreted as not impact-related (included in analysis), adapted from Figure 3 right panel of Robbins & Dones., 2023. The band depth maps are available from the Planetary Data Systems Small Bodies at the following link https://pds-smallbodies.astro.umd.edu/holdings/pds4-nh_derived-v4.0/plutosystem_composition/absorp/.

mechanism due to the presence of conical pits exposing water ice. The non-volatility of water ice indicates that pits have experienced subsurface removal of materials, but differential sublimation may have contributed to pit depth and width (Howard et al., 2017).

In addition, the New Horizons Linear Etalon Imaging Spectral Array (LEISA) instrument together with the Multispectral and Visible Imaging Camera (MVIC) have allowed for the mapping of the spatial distribution of Pluto's surface materials from the acquired infrared spectroscopic data (Grundy et al., 2016). Spectral signature of methane ($CH_4$) is detected on the surrounding uplands and pit rims, while water ice ($H_2O$) signature is present on the floors and lower slopes of some pits, whereas other pits contain more volatile ices, such as nitrogen ($N_2$) signature, which preferentially accumulate in topographic lows (Howard et al., 2017) (Figure 2). Thus, considering the extensivity of similar-sized pit depressions with a close spatial association to linear features, together with their distinctive morphologies, volatile-rich surfaces, incision below the surrounding terrain, and the limitations of previously proposed mechanisms, an endogenic origin is a likely process, possibly due to gaseous effusions from the subsurface (Howard et al., 2017; Moore & Howard, 2021; White et al., 2021).

However, the specific mechanism governing this geological origin and its role in pit formation remains elusive. In this study, we consider the physical characteristics of the pits, including their distribution, planform and cross-sectional morphology, morphometrics (depth, diameter, inner wall slope, rim dimensions), and associations with linear features as geomorphological evidence. We also examine correlations among these physical properties across different pit categorizations such as group type, cross-sectional and planform shapes, which we discuss in



21699100, 2026, 3, Downloaded from https://agupubs.onlinelibrary.wiley.com/doi/10.1029/2025JE009252 by Nasa Goddard, Wiley Online Library on [02/03/2026]. See the Terms and Conditions (https://onlinelibrary.wiley.com/terms-and-conditions) on Wiley Online Library for rules of use; OA articles are governed by the applicable Creative Commons License

21699100, 2026, 3, Downloaded from https://agupubs.onlinelibrary.wiley.com/doi/10.1029/2025JE009252 by Nasa Goddard, Wiley Online Library on [02/03/2026]. See the Terms and Conditions (https://onlinelibrary.wiley.com/terms-and-conditions) on Wiley Online Library for rules of use; OA articles are governed by the applicable Creative Commons License

the context of subsurface fluid-related processes. While we have considered various pit formation mechanisms identified on other planetary bodies (Wyrick & Buczkowski, 2022), the geomorphological evidence in our study area, when taken together with these existing models, leads us to propose an additional process that emphasizes the potential influence of subsurface processes in forming these pits. Here we consider an analogy with Earth's fluid migration, either gas or liquid (Hovland et al., 2002), with resulting insight into Pluto's subsurface dynamics. We propose that pits are forming in a manner analogous to the formation of gas pockmarks in regions with fluid seepage systems on Earth. Observations indicative of a fluid seepage hypothesis focus on the geomorphology and spatial distribution of pits and their relationship to surrounding features. In particular, pit morphology (planform and cross-sectional shapes), clustering patterns, and association with faults may indicate upward migration of subsurface fluids. Similarly on Earth, the morphology and spatial distribution of pockmarks are used as guides for seep detection and exploration of the processes involved (Ceramicola et al., 2018), where circular to elongated depressions commonly manifest as clusters, isolated or chains in relation to fault traces or weakness zones (Hovland et al., 2002). Therefore, if our geomorphological investigation supports our seepage hypothesis, pit distribution could indicate the presence of a volatile reservoir in the subsurface. Thus, our findings could shed light on the subsurface-surface interactions that can contribute to surface-atmosphere volatile transport, ultimately shaping Pluto's landscapes (White et al., 2021), which may also apply to other icy worlds. Given that the impacts of endogenic and exogenic processes on Pluto are not yet fully understood (White et al., 2021), investigating the morphological aspects and depth-to-diameter trends of these pits may help constrain Pluto's subsurface material properties (Singer, Greenstreet, et al., 2021).

In this study, we characterized and measured pit dimensions in the study area using the Java Mission-planning and Analysis for Remote Sensing (JMARS v.5.3.0) software (Christensen et al., 2009) to analyze pit morphology and distribution. Through a comparative planetology approach, drawing on terrestrial analogs where fluid seepage, fault-controlled migration pathways, and pit morphologies are well studied (e.g., Chuvilin et al., 2020; Dandapath et al., 2010; Gafeira et al., 2018; Omeru et al., 2021; Szpak et al., 2015), we interpret the geomorphological expressions observed in Pluto's pits. Our correlation studies between the depth and diameter of pits and geomorphological observations of the pits based on their cross-sectional and planform views and their overall planform distribution and surrounding linear features indicate a close association between pits, faults, and slope variations, likely related to fluid escape and emission. Since faults may act either as conduits or barriers (Pei et al., 2015) to subsurface fluid migration on terrestrial fluid seepage systems, we examine their apparent spatial relationship to pits, their length and interpreted surface relief across the fault traces, and local slope changes. These attributes allow us to assess whether faults may have influenced pit formation on Pluto. Our findings suggest that while faults appear to act as a conduit for subsurface fluid migration and thus influence pit formation, they may not consistently act as conduits for fluid migration. These findings suggest that a combination of structural controls and surface processes influences pit formation on Pluto, warranting further investigation into potential subsurface reservoirs and volatile release mechanisms.

## 2. Methods

We analyzed each of the pits and linear features in the studied region within Pioneer Terra, the northeast region of Sputnik Planitia (Figure 1), using the global mosaic and digital elevation model (DEM) (~300 m/pixel respectively) (Schenk et al., 2018) within JMARS. The DEM is able to resolve for features with estimated vertical precision as low as ~100 m (Schenk et al., 2018). The average pit diameter in our data set is 3.88 km, which is equivalent to ~13 pixels in the global mosaic, while the average pit depth is 0.55 km, which is equivalent to ~2 pixels in the global DEM. Since measurements were done approaching the resolution limit, the numbers here are best interpreted as lower limits. Pits with depth less than 300 m or less than 1 pixel are flagged as low-confidence measurements (Table S1). Pits interpreted as possible impact craters were excluded from the analysis (see Figure 3 right panel of Robbins & Dones, 2023). Cylindrical map projections centered on 180° longitude were used for both global DEM and mosaic within JMARS. We analyzed the surface composition of the study area using QGIS (v.3.40.5-Bratislava) (QGIS Development Team, 2022) (Figure 2) and the spatial distribution of pits in the study area using Tableau Desktop (Professional Edition, 2024.2.2), (2024). Statistical analysis and visualization were created using Visual Studio Code (v.1.96.4), (2024).

Pits were identified visually and subsequently confirmed using four to six topographic profiles to define their extent by tying feature edges to inversion points in the topography when identifying pits (see Figure 4 of Singer, McKinnon & Schenk, 2021). For pits that are conjoined in a linear manner forming a pit chain, six topographic

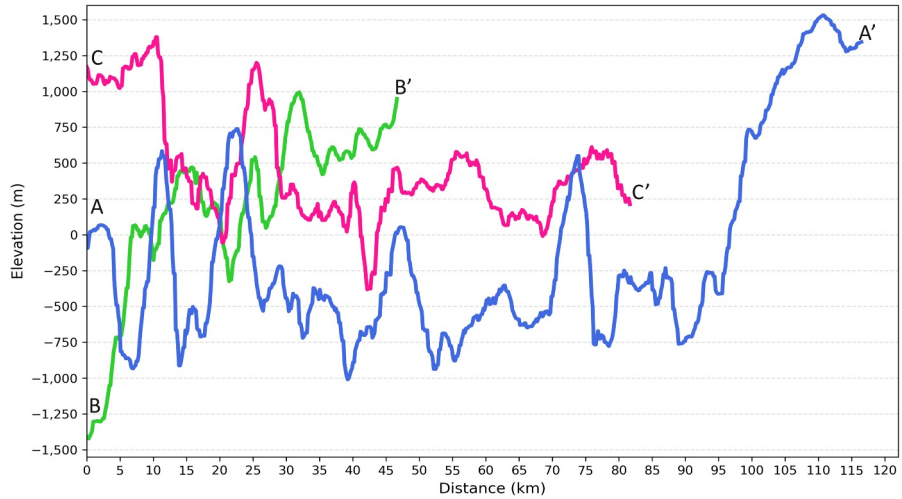


**Figure 3.** Topographic profiles were extracted along three fault-associated pit chains in the study region. Fault A is shown in blue (vertical exaggeration ≈ 46x), Fault B in green (vertical exaggeration ≈ 19x), and Fault C in pink (vertical exaggeration ≈ 46x). The locations of all three profile paths are displayed in Figure 1. In this region, faults manifest as pit chains (McGovern et al., 2021), and the depressions in each profile represent pits along the fault traces. Profiles show varying slopes and lengths from west to east. (A-A′) Fault A progresses longer and deeper, with the lowest elevation at ∼1 km. (C-C′) Fault C's lowest elevation is half of Fault A at ∼0.5 km. (B-B′) Fault B has the shortest distance with an upslope direction, coinciding with the shortest pit chain (see Figure 1) when compared to Faults A and C.

profiles, each approximately 0.5–1 km in length, are drawn along the pit chain, from which the most representative profile was selected (Figure S1 in Supporting Information S1). The profile showing the most depressions in accordance with the mosaic overlaid by the colorized shaded relief layer (Moore et al., 2016) and the deepest depressions based on the darker regions of the DEM is taken as the base profile to account for the pits in the chain. If the topographic profiles with the most depressions and the deepest depressions do not overlap, a middle topographic profile is drawn to capture the overall averaged pit chain profiles (Figure S1 in Supporting Information S1). Each pit diameter is determined by identifying the feature edges on both sides, which are defined by a break in slope or an inversion point in the topography, that is, where the steep slope of the pit wall meets the shallower or flat surrounding terrain (Singer, McKinnon & Schenk, 2021), and measuring the distance between them (Figure S1 in Supporting Information S1). For pit chains, it is challenging to discern the edge as they share walls; therefore, the edge is taken where the deeper region in the DEM and shaded relief coincides with the individual pit edges. Minor axis lines, the shortest length of the pit, are drawn perpendicular to the topographic profile representing the major axis, the longest length of the pit (Figure S1 in Supporting Information S1). For pits that are visually more challenging to discern, the minor axis is drawn perpendicularly at the deepest part of the major axis.

Once the edges are identified, the highest elevation of the edge is subtracted from the lowest elevation of the pit profile to obtain the overall depth of the pit depression (Figure S1 in Supporting Information S1). The slope of the inner wall is taken as the ratio of vertical elevation difference, $\Delta z$, and distance from the highest to the lowest point of each wall of the pit edge, $\Delta x$ (Figure S1 in Supporting Information S1). While the rim width can be difficult to distinguish, we measured the rim width from the interpreted pit edge, past the inversion point at the highest elevation of the pit-shaped profile into shallower or flat surrounding terrain or neighboring pit or mound, to the lowest elevation before the slope breaks into a higher mound, lower neighboring pit, or flat surrounding terrain. The rim height is the elevation of the highest point between the interpreted rim width and the pit edge subtracted from the elevation of the interpreted pit edge (Figure S1 in Supporting Information S1).

The pits were classified based on planform view into group types: clusters, chains, and isolated pits (Ceramicola et al., 2018), and based on cross-sectional shapes of their major axis: V, U (>1 km base diameter), and W (Andresen et al., 2008). The major and minor axis ratios were used to classify them into circular (1–1.5), elliptical (1.5–2.5), and elongated (≥2.5) (K. Zhang et al., 2020). Similar classification methods and criteria for pits were also employed on Earth (e.g., Dandapath et al., 2010; Gafeira et al., 2018; Omeru et al., 2021; Szpak et al., 2015). The Radial Profiling Tool in the Crater Counting Layer was further used to determine the steepest wall orientation



21699100, 2026, 3, Downloaded from https://agupubs.onlinelibrary.wiley.com/doi/10.1029/2025JE009252 by Nasa Goddard, Wiley Online Library on [02/03/2026]. See the Terms and Conditions (https://onlinelibrary.wiley.com/terms-and-conditions) on Wiley Online Library for rules of use; OA articles are governed by the applicable Creative Commons License

(Table S1). Vertical exaggeration for all topographic profiles was calculated directly from the ratio of the plotted horizontal distance range to the plotted vertical range displayed in the JMARS profile chart. We report the vertical exaggeration values for each profile in the corresponding figure captions. All profiles were extracted at the maximum available JMARS resolution (in pixels per degree).

## 3. Results

### 3.1. Geomorphological Observation

A widespread occurrence of pits with close spatial association to structural lineations interpreted as faults has been identified in Pioneer Terra (Howard et al., 2017; McGovern et al., 2021). A total of 150 pits, in this study, have been identified and characterized by morphologies in terms of (a) planform distribution, (b) cross-sectional shape in the topographic profile, and (c) planform shape based on major and minor axis ratios. The pits' location, characteristics, and dimensions are listed in Table S1 with an average diameter of ∼3.88 km ± 0.88 km and an average depth of ∼0.55 km ± 0.15 km. We observe tectonic lineations that are continuous and connected to the pits forming longer pit chains (Figure 1). Of particular interest are the two major tectonic lineations, Faults A and C, which exhibit the highest pit density in the region of interest, and a minor fault, Fault B, located at the eastern side of the largest impact crater in the study area (Figure 1). Fault A is interpreted here as a major fault based on similar geomorphology to the southern major fault, Fault C (i.e., both faults manifest as pit chains oriented NW–SE), which has been interpreted as an extensional fault by prior works (Keane et al., 2016; McGovern et al., 2021).

When examining the pits from a planform view, the pits generally appear concentrated on the southern side of Faults A and C (white arrows in Figure 1), although minor pit densities also occur on the north and western sides of Fault A (Figure 1). The highest pit density coinciding with Fault A is located closer to the smooth uplands terrain described by Howard et al. (2017), where the broad depressions in that region are considered as the source of the upland mantles (Howard et al., 2017). We observed two clusters of pit occurrences associated with the southern side of Fault A (Figure 1). On the left side, larger pits with a more rugose appearance are observed, while the right side features a collapsed-looking structure composed of an abundance of smaller and shallower pits relative to the surrounding pits.

When the study area shown (Figure 1) is compared to the spectral map (Figure 2), the water-rich ice spectral signature is concentrated in part of the northern rugose pit cluster, across all three faults, and pit clusters observed on Fault C. An $N_2$-rich ice signature is more prominent in the collapsed-looking pit cluster associated with Fault A, including the western and southwestern sides of Fault A, and in the floor of the largest impact crater in the study area (Howard et al., 2017). Pits tend to be larger and deeper in the water-rich ice areas compared to the $N_2$-rich ice region, suggesting that the presence of volatile ice strongly influences the observed topographic features (Hedgepeth et al., 2023).

When comparing the fault profiles', we observe that the length, slope (Figure 3), and width (Figure 4) of faults appear to influence the pit distribution as the highest pit density occurs in close spatial association with Faults A and C (Figure 1).

The topographic undulations observed in the elevation profile across the study area (Figure 4) show an abundance of relatively shallow pit-like depressions on the southern side of the study area, in contrast to the northern side. The major dips in the profiles in Figure 4 correspond to the faults and pits present in the region. In the profile, pits appear as shallower depressions, whereas fault-related offsets, often manifesting as pit chains, produce more abrupt elevation drops. A raised rim occurs on each side between each fault zone boundary (vertical black arrows). Raised rims are interpreted as local elevation highs that occur immediately before the downward slope into each pit depression. Raised rims, topographic highs, or mound-like features have been observed with “pockmark” -like features in terrestrial settings, forming linear chains along faults and are often associated with fluid seepage structures clustered along fault zones (Kluesner et al., 2013). The absence of such a feature in between of Fault B may reflect limited fluid migration along that segment, which could explain the relatively fewer pits observed between the three faults. All three fault boundaries display a consistent upslope direction across the faults, following the regional upslope direction in Figure 4.



21699100, 2026, 3, Downloaded from https://agupubs.onlinelibrary.wiley.com/doi/10.1029/2025JE009252 by Nasa Goddard, Wiley Online Library on [02/03/2026]. See the Terms and Conditions (https://onlinelibrary.wiley.com/terms-and-conditions) on Wiley Online Library for rules of use; OA articles are governed by the applicable Creative Commons License

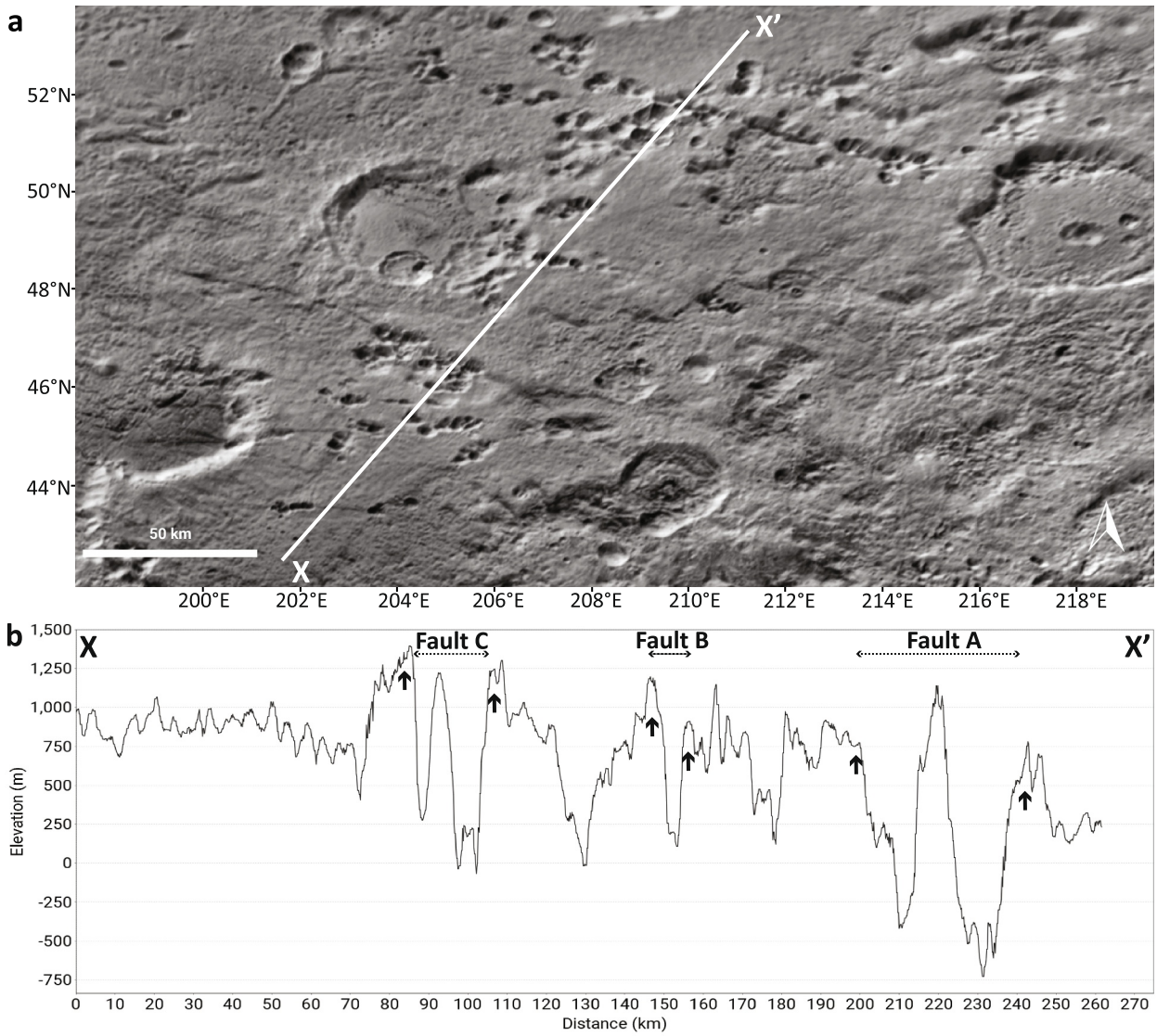


**Figure 4.** (a) Global mosaic of the study area with the X-X′ elevation profile path, profile is displayed in the bottom panel (vertical exaggeration ≈ 120x). (b) The elevation profile across the study area reveals a regional slope that trends upslope from north to south. Boundaries of fault zones A, B, and C are shown along the X-X′ transect, with interpreted raised rims appearing on each side (vertical black arrows). A topographic high (i.e., a mound-like feature) appears between zones of Faults A and C but not Fault B.

### 3.2. Pit Distribution and Morphology

To constrain the nature of pits in the region, we performed correlation studies between the measured morphologic parameters, following approaches used in terrestrial pockmark work (e.g., Audsley et al., 2019; Sun et al., 2011; K. Zhang et al., 2020; Z. Zhang et al., 2021). The pits observed on Pluto share key morphological traits with terrestrial gas pockmarks, including their circular to elliptical planforms that can be up to kilometers in diameter (Sun et al., 2011), clustered and chained distributions (Ceramicola et al., 2018), U- to W-shaped pits (Andresen et al., 2008; Gupta & Micallef, 2023), and sometimes with raised rims (Forwick et al., 2009). These morphological similarities and the spatial relationship of pits with faults (see Section 3.1) suggest a possible shared formation mechanism, where subsurface fluid release could drive the formation of pits on Pluto's surface analogous to gas pockmark formation on Earth. The distribution, morphology, and trend in depth versus diameter of each pit are discussed in terms of the implications of subsurface fluid flow.

We identified key statistical relationships between depth-to-diameter plots based on (a) group type, (b) planform shape, and (c) cross-sectional shape-dependent trends (Figures 5b–5d). The pits can be classified into chain



21699100, 2026, 3, Downloaded from https://agupubs.onlinelibrary.wiley.com/doi/10.1029/2025JE009252 by Nasa Goddard, Wiley Online Library on [02/03/2026]. See the Terms and Conditions (https://onlinelibrary.wiley.com/terms-and-conditions) on Wiley Online Library for rules of use; OA articles are governed by the applicable Creative Commons License

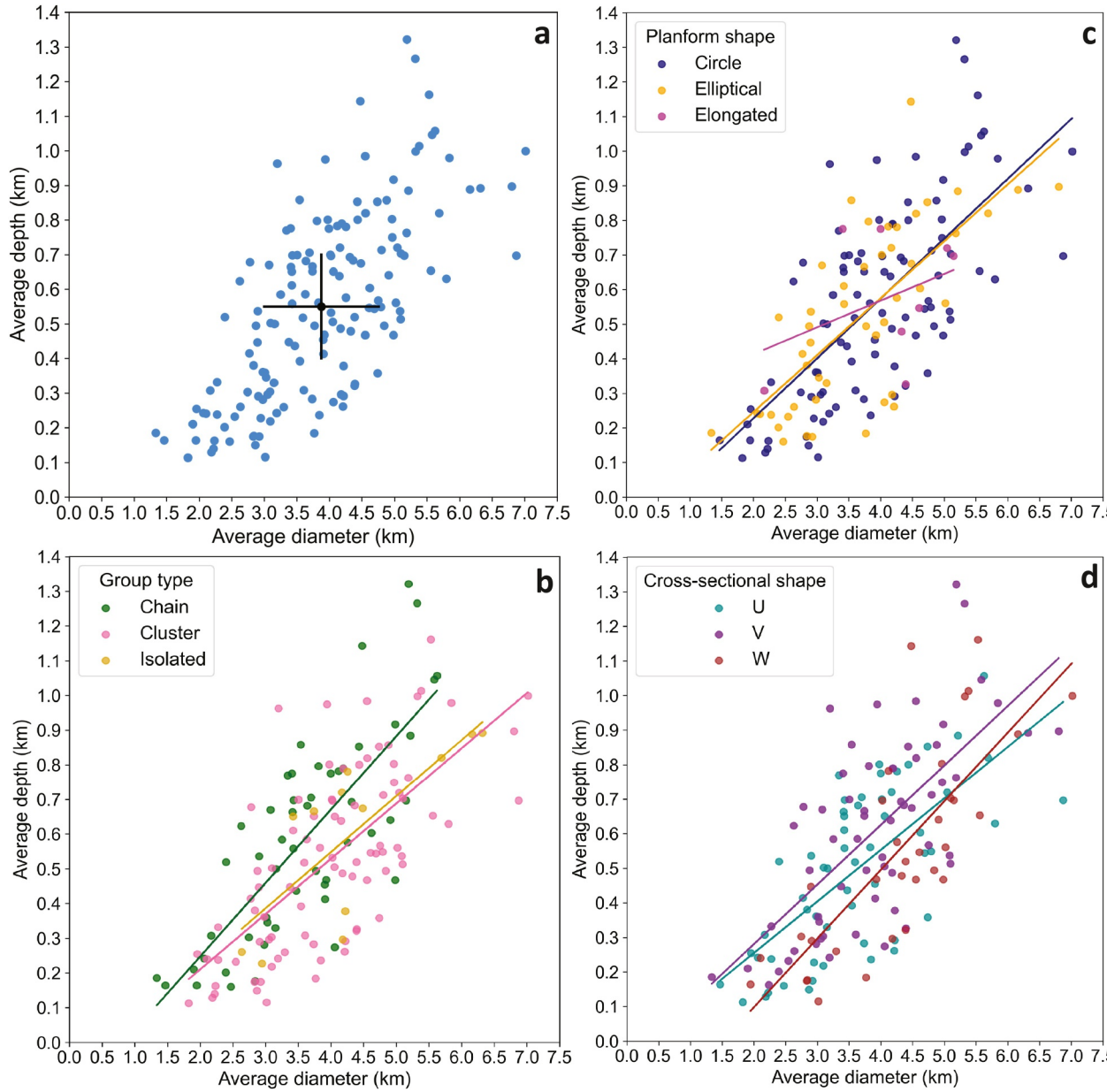


**Figure 5.** (a) Correlation studies between average depth and average diameter of pits in the study area with error bars showing 1-$\sigma$ uncertainty from mean average depth and diameter. In total, the average diameter of these pits ranges from 1.3 to 7 km, with a mean of ∼3.88 km, median of ∼3.91 km, and standard deviation of ∼0.88 km. The average depth of pits ranged from 0.11 to 1.32 km, with a mean of ∼0.55 km, median of ∼0.54 km, and standard deviation of ∼0.15 km. Correlation studies of all pits in (a) are categorized into (b) group type in planform view, (c) pit shape based on the major and minor axis ratio, and (d) cross-sectional shape of the major axis. Lines in panels (b)–(d) represent best-fit linear regressions computed using ordinary least squares.

(35%), cluster (57%), and isolated (8%). Notably, pit chains exhibit the highest depth to diameter correlation ($R^2 = 0.598$) among the three group types, which may suggest a relatively more uniform formation mechanism, possibly linked to pre-existing structural controls. In this context, higher $R^2$ values indicate that a larger fraction of the variance in pit depth is explained by pit diameter, reflecting a stronger linear relationship and lesser scatter comparatively. Although all $R^2$ values fall within the moderate range (Table 1), the pit chain relationship is statistically meaningful because it is supported by a substantial sample size ($n = 52$). Isolated pits show approximately similar $R^2$ values but are represented by far fewer measurements ($n = 12$), making their relationship less statistically robust. Pits occurring in clusters exhibit a relatively lower $R^2$ value, reflecting greater scatter and weaker depth to diameter relationship. All three group types indicate that the larger pits generally have



21699100, 2026, 3, Downloaded from https://agupubs.onlinelibrary.wiley.com/doi/10.1029/2025JE009252 by Nasa Goddard, Wiley Online Library on [02/03/2026]. See the Terms and Conditions (https://onlinelibrary.wiley.com/terms-and-conditions) on Wiley Online Library for rules of use; OA articles are governed by the applicable Creative Commons License

**Table 1**
*Coefficient of Determination ($R^2$) Values for Average Diameter-Depth Linear Regressions for All Three Classification Schemes Evaluated in This Study: Group Type, Planform Shape, and Cross-Sectional Shape*

| Classification | Category | $R^2$ | Number of pits |
|---|---|---|---|
| Group type | Chain | 0.5982 | 52 |
| | Cluster | 0.4816 | 86 |
| | Isolated | 0.5928 | 12 |
| Planform shape | Circle | 0.4834 | 94 |
| | Elliptical | 0.5193 | 48 |
| | Elongated | 0.1518 | 8 |
| Cross-sectional shape | U | 0.4744 | 56 |
| | V | 0.4596 | 60 |
| | W | 0.6032 | 34 |

*Note.* Each row lists the three subcategories within each classification along with their corresponding $R^2$ values. The number of pits in each subcategory is listed in the rightmost column.

deeper depressions although this relationship is not consistent throughout the study area. In contrast, pits formed due to diapirism and melting on Europa display a more systematic correlation between diameter and depth, where larger pits are consistently deeper than smaller ones, possibly due to greater volume loss associated with larger diapirs (Singer, McKinnon & Schenk, 2021).

The major and minor axis ratios of pits were used to classify the pits into circular (63%), elliptical (32%), or elongated (5%). Circular pits exhibit the largest average diameter and depth among pit shapes and show a moderate positive correlation ($R^2 = 0.4834$) between these properties, unlike terrestrial studies where such a trend is often weak or absent (e.g., Sun et al., 2011; K. Zhang et al., 2020; Z. Zhang et al., 2021). This implies that Pluto's circular pits may be primarily controlled by localized subsurface gas release, maintaining their radial symmetry due to sustained venting rather than a single fluid expulsion event. On Earth, circular pockmarks can evolve into elliptical or elongated forms through erosion and current-driven processes, indicating that pockmarks are not recent formation (Andresen et al., 2008); however, since Pluto lacks liquid-driven erosion, other mechanisms such as sublimation may play a role in modifying pit shapes over time (Howard et al., 2017), suggesting that the studied pits may have undergone long-term evolution. Elongated pits exhibit a weaker correlation at $R^2 = 0.152$ (Table 1), possibly due to low sample size, although similar depth-to-diameter relationships have been observed for elongated pockmarks on Earth (Z. Zhang et al., 2021).

The cross-sectional shapes of pits are classified into U-shaped (37%), V-shaped (40%), and W-shaped (23%) based on the interior topography of pit profiles. In terms of diameter, W-shaped pits are the largest, followed by U-shaped and V-shaped pits. However, this trend does not hold for pit depth. Despite these variations, all three shape categories show a positive correlation between depth and diameter, with the W-shaped pits showing the highest correlation at $R^2 = 0.603$ (Table 1). W-shaped pockmarks on Earth are often linked to active gas venting and sediment fluidization (Gupta & Micallef, 2023). The presence of these features may indicate ongoing or past subsurface gas escape though additional evidence is required to confirm this.

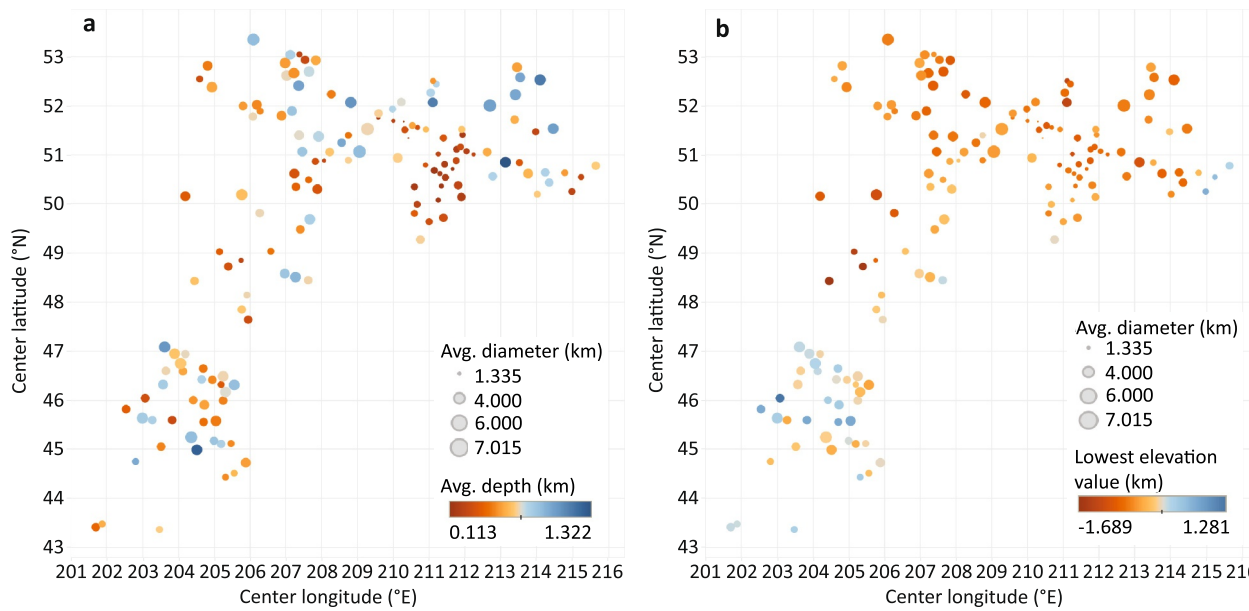


**Figure 6.** The spatial distribution of pits in the study area where axes latitude and longitude indicate the approximate centroid of each pit (see Figure 1). Bubble size represents the average diameter of each pit, while the color represents (a) the average depth of each pit and (b) the lowest elevation value of each pit.



21699100, 2026, 3, Downloaded from https://agupubs.onlinelibrary.wiley.com/doi/10.1029/2025JE009252 by Nasa Goddard, Wiley Online Library on [02/03/2026]. See the Terms and Conditions (https://onlinelibrary.wiley.com/terms-and-conditions) on Wiley Online Library for rules of use; OA articles are governed by the applicable Creative Commons License

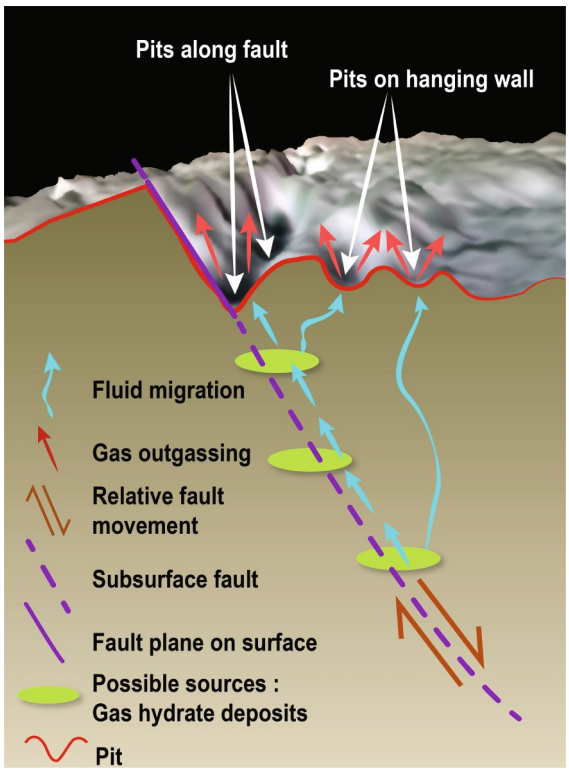


**Figure 7.** Conceptual model showing pits forming along the fault through fluid migration represented by small blue arrows. Pits also form on downthrown blocks, where fluid seepage, represented by longer blue arrows, results from volume imbalance and excess fluid pressure in the subsurface. A portion of the 3D layer of the study area is taken from the global digital elevation model in JMARS, with a display vertical exaggeration of 7.

Our results show that the majority of pits with the lowest values of average depth are primarily concentrated between latitudes 48°N and 53°N and longitudes 208°E and 212°E, while pits with the lowest elevation values appear to be concentrated between latitudes 48°N and 53°N and longitudes 204°E and 214°E approximately (Figure 6). This implies that the lowest elevation value for each pit is associated with latitude, consistent with the distribution of pits with the shallowest depth and smallest diameter, where an upslope direction from the northern to southern side of the study area is observed (Figure 4). The lowest elevation values are also concentrated in zones of weakness, such as the faults, and within the only largest impact crater, relative to the surrounding pits.

## 4. Discussion

### 4.1. Fluid Seepage Conditions and Pit Formation

Considering similar systems producing fluid-expulsion craters on Earth may be a key to understanding the origin of these pits. The existence of a fluid seep system on Earth requires three main structural elements to be present: (a) fluid source, (b) plumbing system, and (c) surface manifestation of seeping features at or near the surface (Talukder, 2012). Seeping features such as gas pockmarks vary in size, shape, and distribution depending on geological controls such as fault systems, subsurface lithology, and fluid fluxes (Hovland et al., 2002). Terrestrial pockmark diameter and depth typically have a positive correlation and scale linearly since both are correlated with the magnitude of fluid seepage events (Batchelor et al., 2022). In our correlation studies discussed in Section 3.2, similar linear trends were observed for the pit depth and diameter in this work (Figure 5). Additionally, we observed a latitudinal correlation between the lowest pit elevation and average pit dimensions (Figure 6) as well as spatial correlations between fault dimensions and pit distribution (Figures 1, 3 and 4). These trends and observations suggest that potential influences from subsurface processes and surface modification mechanisms may be shaping these pits within Pioneer Terra.

Based on the depth-to-diameter relationships and geomorphological observations in the studied region, we propose a two-stage process of pit formation, analogous to a source-reservoir-seal fluid migration system (Z. Zhang et al., 2021). Stage 1: Gas hydrate dissociation due to environmental changes results in fluid-bearing gas escape, forming pits along and across faults (Figure 7). Stage 2: Continued gas leakage, slope deformation, and sublimation processes modify pit morphology.

Drawing parallels from Earth's seepage systems and associated features, we discuss the main structural components when exploring potential fluid seepage on Pluto. Fluid sources for a seep system can either be abiogenic or thermogenic in nature (Oehler & Etiope, 2017) and may originate from deep sources (Z. Zhang et al., 2021). On Pluto, abiotic methane could be produced from water-rock reactions if interior water oceans existed (Grundy et al., 2024), where serpentinization reactions in the interior would drive vent chemistry producing $H_2$, $CH_4$, and other hydrocarbons (Hand et al., 2020). Thermogenic methane has been proposed for Pluto (Kamata et al., 2019) and is derived from the decomposition of organic materials from their organic-rich cores (McKinnon et al., 2020). $CH_4$ is preferentially trapped in clathrate hydrates as compared to $N_2$ (Courville et al., 2023) or CO (McKinnon et al., 2020) and is predicted near Pluto's surface (Courville et al., 2023). Up to ~13 km of $CH_4$ clathrate layer may have formed on Pluto (Carnahan et al., 2022), supporting the consideration of gas hydrate deposits as a possible fluid source when evaluating the fluid seepage hypothesis. Theoretical models suggest that near-surface crustal deposits could lead to hydrate emissions through seeps (Boström et al., 2021) (Figure 7).

On Earth, methane migration into the Gas Hydrate Stability Zone (GHSZ) via fracture systems is constrained by a stress state, and the interactions between stress and permeability influence hydrate formation and the heterogeneous distribution of hydrate across spatial scales (Weinberger & Brown, 2006). Gas hydrates formed during the migration of thermogenic gas into the GHSZ may dissociate to form gas pockmarks (Batchelor et al., 2022).



21699100, 2026, 3, Downloaded from https://agupubs.onlinelibrary.wiley.com/doi/10.1029/2025JE009252 by Nasa Goddard, Wiley Online Library on [02/03/2026]. See the Terms and Conditions (https://onlinelibrary.wiley.com/terms-and-conditions) on Wiley Online Library for rules of use; OA articles are governed by the applicable Creative Commons License

21699100, 2026, 3, Downloaded from https://agupubs.onlinelibrary.wiley.com/doi/10.1029/2025JE009252 by Nasa Goddard, Wiley Online Library on [02/03/2026]. See the Terms and Conditions (https://onlinelibrary.wiley.com/terms-and-conditions) on Wiley Online Library for rules of use; OA articles are governed by the applicable Creative Commons License

Hence, the presence and distribution of pockmarks may indicate the presence and distribution of gas hydrate in that locale (Z. Zhang et al., 2021). Relict or metastable gas hydrates found within 200 m depth in permafrost regions can remain self-preserved depending on temperature, salinity, ice content, and gas pressure (Chuvilin et al., 2018), but climate variation could trigger large gas venting from underlying dissociating hydrate deposits (Frederick & Buffett, 2014). Elevation and slope variations in this studied region may indicate a complex icy stratigraphy on Pluto (Figures 3 and 4), where stratigraphic gas hydrate traps could exist. Given that the study area falls within a permanent tropical arctic region of Pluto (see Table 1 of Binzel et al., 2017), this region of Pluto may experience maximum cyclical extremes causing variation in pressure and temperature conditions. The temperature and pressure changes could likely trigger the dissociation of gas hydrates under ideal conditions, leading to episodic gas release events forming pits (Figure 7). Hydrate dissociation as the source of gas outgassing has been proposed to occur on Mars (Oehler & Etiope, 2017) and Titan (Tobie et al., 2006).

Plumbing systems can be either structural, stratigraphical, or both, allowing for fluid migration (Talukder, 2012). Fluid migration routes aiding seepage occur preferentially through permeable pathways or lineaments such as joints, faults/fractures, and breaches in the overlying lithology (Oehler & Etiope, 2017), representing zones of weakness in a planet's crust (Enoh et al., 2021). Faults can act as both conduits and seals or barriers (Pei et al., 2015), simultaneously facilitating and restricting fluid flow (Cawood et al., 2024). Additionally, high porosity lithologies can allow gas to seep through gas chimneys that originate at the top of shallow gas pockets on Earth (Cathles et al., 2010). On Pluto, despite the transition of faults from loading-to TPW-dominated, the NW–SE extensional faults in the study area remain consistent regardless of the stress source (Keane et al., 2016), which could guide long-term subsurface-surface fluid migration (Figure 7). Given the implications of low thermal inertia on the surface of Pluto, indicating high surface porosity and poor consolidation (Lellouch et al., 2011), Pluto may also exhibit conditions that allow for fluid seepage to occur through overlying ice in addition to the presence of faults (Figure 7).

On Earth, when faults act as conduits, gas pockmarks often form directly on faults and the hanging wall of an extensional fault (Q. Zhang et al., 2025). However, if volatiles escape the upper tip of faults, pockmarks may align with the fault strike regardless of their distance from the fault (Q. Zhang et al., 2025). Conversely, if faults act as seals, fluid migration can still occur due to volume imbalance when fluid pressure increases relative to the overburden pressure (Pilcher & Argent, 2007). The resulting over-pressured fluid deposits may drive vertical migration from the footwall or fault, forming pockmarks on the downthrown hanging wall (Pilcher & Argent, 2007; Q. Zhang et al., 2025). Furthermore, gas hydrates may also play a role in fault sealing capacities, forming compartmentalization of subsurface gas reservoirs (Madrussani et al., 2010), and thus influencing the distribution of gas pockmarks. Small-offset faults are also commonly identified below gas pockmarks on Earth (Strozyk et al., 2018), and directional fault trends are critical factors in determining seepage flow (Enoh et al., 2021). Therefore, fault mapping and analysis of associated geometries should be prioritized to assess leakage potential (Cawood et al., 2024).

Building on this foundation, the role of extensional faults may have influenced the distribution of pits in this localized region of Pioneer Terra. Fault C, being shorter, narrower, and shallower in terms of surface relief, corresponds to a lower pit density, suggesting a lesser volume imbalance and lower fluid pressure relative to Fault A (Figures 1, 3 and 4). In contrast, the higher pit density on and near the longer, deeper, and broader surface relief of Fault A may result from greater volume imbalances requiring compensation, leading to lateral pit growth and longer pit chains (Figures 1, 3, 4 and 7). Fault C is interpreted to act more as a seal, as pits appear only on the downthrown block of the extensional fault, while Fault A seems to function as both a seal and a conduit, with pits appearing on the downthrown blocks and, to a lesser extent, on the upthrown blocks (Figure 1). We note that while pits occur predominantly on the southern side, the topographic profile indicates higher terrain on the south of the fault zone (Figure 4). This may reflect secondary processes such as volatile deposition affecting asymmetric erosion rather than fault kinematics alone. Fault A acting as a fluid conduit may also explain the higher abundance of pit density in the study area (Figures 1 and 7). Microfractures beyond the resolution of available data could also facilitate fluid migration. Fully resolving the structural configuration would require detailed structural modeling and higher resolution stratigraphic or compositional data, which are beyond the scope of this study but represent promising avenues for future work.

21699100, 2026, 3, Downloaded from https://agupubs.onlinelibrary.wiley.com/doi/10.1029/2025JE009252 by Nasa Goddard, Wiley Online Library on [02/03/2026]. See the Terms and Conditions (https://onlinelibrary.wiley.com/terms-and-conditions) on Wiley Online Library for rules of use; OA articles are governed by the applicable Creative Commons License

### 4.2. Controls on Pit Modification

On Earth, pockmark chains or gullies tend to form downslope in the direction of fault movement due to gravitational slumping in unstable areas, sometimes coalescing into clustered, amalgamated depressions (Pilcher & Argent, 2007). Meanwhile, upslope pockmark development can trigger slumping and material sliding, thus widening pockmark gullies (Cronin & Jubilee Team, 2022). The occurrence of hydrate reservoirs may also trigger large slope failures and events of sediment collapse (Hovland, 2012). This could explain why pockmarks tend to be more widely distributed in areas with slope instability, possibly due to local overloading and subsequent dissociation of hydrates (Loncke et al., 2004).

For this reason, regional and localized slope variations along and across the two major faults, Fault A and C, as well as the minor fault, Fault B, may influence the localized distribution and modification of pits, influencing density, dimensions, and group type (Figure 1). The regional slope of the study area transitions from downslope in the north to upslope in the south (Figure 4). However, the pit chains and clusters predominantly occur along the direction of extensional fault movement (Figures 1 and 7). Meanwhile, the upslope regional gradient may be contributing to material instability and collapse on the southern (upslope) side of the pit, which could explain why a majority of the pits exhibit pronounced steepening of their northern wall sections (Table S1).

On Pluto, variations in crustal ice composition and thickness may also be influenced by volatile removal processes such as sublimation (Moore et al., 2017) and seasonal changes in volatiles (Earle et al., 2017) that may have influenced physical and chemical processes over time. For instance, Fault A's $N_2$-rich ice collapsed-looking feature (Howard et al., 2017) on the northern side of the study area contains the smallest and shallowest pits (Figure 6), consistent with expectations that high viscosity strata limit heat flow to the surface (Boström et al., 2021), resulting in smaller pit dimensions. Besides impacting the mechanical strength of pits, volatile variations on Pluto may also influence fault dip angle changes (Kling et al., 2021) and diagenetic processes affecting fault sealing capacity (Pei et al., 2015). As a result, fluid migration from the subsurface and subsequent pit formation and modification are likely to change based on seasonal variation, supporting our notion that the studied pits may have undergone long-term evolution. It remains uncertain whether surrounding fluid expulsion events never occurred due to unfavorable environmental influence in the subsurface and/or surface, or whether surface manifestations of seepage activity were entirely removed due to surficial processes such as differential deposition of materials (Moore et al., 2016).

Although terrestrial pockmarks are significantly smaller than Pluto's pits, the scale difference may reflect contrasts in substrate strength and mechanics, gravity, and volatile storage capacity. The larger scale of Pluto's pits may result from enhanced volatile accumulation in an ice-rich crust, lower gravity permitting broader collapse, or long-term interaction with subsurface fracture systems, while terrestrial pockmarks typically involve shallow sediment deformation or form in unconsolidated marine sediments under high overburden pressure. Our use of terrestrial analogs is therefore morphological and conceptual rather than implying a direct physical scaling. Permafrost-related collapsed pits provide a closer analog in terms of thermal environment and substrate mechanics, reinforcing the interpretation that fluid migration and expulsion can generate rimmed depressions in cold, ice-rich materials. Finally, subsurface-to-surface volatile transport along fractures on Pluto has been proposed in several recent studies (Cruikshank et al., 2019, 2021; Dalle Ore et al., 2019; Howard et al., 2023; C. R. Martin & Binzel, 2021; Singer et al., 2022), supporting the broader premise that the pits may reflect fluid seepage along structurally controlled lineaments.

### 4.3. Implications and Future Work

Various geomorphological features hint at the possibility of subsurface fluid migration and seepage events in forming the pits in our study area within Pioneer Terra. These observations support previous interpretations of endogenic processes forming pits in this region (Howard et al., 2017; Moore & Howard, 2021; White et al., 2021) and provide additional insight into the interplay between subsurface processes and pit formation on Pluto.

While a more extensive modeling approach is required to corroborate the pit formation mechanisms, our findings provide preliminary insights into assessing the plausibility of our fluid seepage hypothesis. Through a comparative planetology approach, we presented geomorphological observations of pits and associated faults, indicating the influence of slope, latitudinal, and volatile variations on pit distribution within our study area. We characterized the pits according to group type, planform, and cross-sectional shape, and conducted correlation studies to

observe how the morphology and depth-to-diameter trends for each classification compared with those observed for gas pockmarks on Earth. Based on the main structural conditions required for seep systems, we developed a conceptual model to propose possible pathways for pit formation via fluid migration and seepage.

The likely presence of gas hydrates near the surface of Pluto (Courville et al., 2023) could destabilize to be a source of gas seepage forming pits as emission points. Gas species similar to methane can both be sequestered and released from gas hydrate dissociation, which increases the likelihood of freed gasses contributing to greenhouse gasses and atmospheric constituents if they reach the atmosphere (Kvenvolden, 1993). On Earth, the global contribution of greenhouse gases can be substantial, despite the small amount of gas released from a single pockmark (Gupta et al., 2022), similar to the phenomenon proposed on Mars, where just a few seeps can sustain the atmospheric $CH_4$ level (Etiope et al., 2013). Pluto's seasonal volatile changes (Earle et al., 2017) may periodically alter the volatile inventory of near-surface reservoirs. Because the characteristics of pits are proposed to be influenced by the conditions and availability of subsurface volatile reservoirs, this study highlights potential links between Pluto's surface and subsurface conditions as well as its atmospheric processes. Understanding how the pits evolve over time and under different seasonal conditions will be crucial for determining whether Pluto's subsurface conditions can host transient or long-term volatile storage. These findings open new avenues for future research into subsurface-surface-atmosphere interactions on Pluto.

Several lines of inquiry into the nature of fluid sources, reservoirs, and migration routes that emerged from this study are promising subjects for future work. Specifically, the relationship between pit characteristics, fluid source, reservoir characterization, and fault systems can further elucidate subsurface dynamics and properties of Pluto. Several key mechanistic questions remain open. (a) What volatile species (e.g., $N_2$, $CH_4$, $H_2O$, $NH_3$ hydrates) are most plausible in Pluto's upper crust, and under what pressure-temperature conditions could they accumulate, mobilize, and dissociate to form pits? (b) Do these volatiles migrate gradually along permeable fractures, or episodically or catastrophically as pressure builds beneath an impermeable layer? (c) What is the physical and chemical state of the icy crust required for pit formation, and might the putative subsurface ocean influence fracture propagation or volatile accumulation? While modeling work is outside the scope of this geomorphological study, future research could incorporate our morphometric input (Table S1) and observations for more comprehensive statistical analyses and models to validate the existence of these interactions and to develop more detailed mechanistic hypotheses. The modeling of fluid sources and simulations of fluid seepage may yield further insights into other ambiguous features and help refine climate models for Pluto and other icy worlds.

## 5. Conclusions

The physical characteristics of Pluto's pits in Pioneer Terra suggest that the features may be analogous to terrestrial gas pockmarks. Together, the distribution and morphologies of pits with close spatial associations to faults could potentially be explained by fluid migration and seepage from the subsurface. We propose that the dissociation of gas hydrate deposits could likely be the fluid source in forming pits that may act as localized discharge points for gasses such as methane. Even minor episodic releases may contribute to atmospheric constituents if they reach the atmosphere; thus, a comprehensive understanding of the dissociation of subsurface hydrates and their feedback interaction with surface geomorphology and potential contribution to the atmosphere is essential for elucidating Pluto's atmospheric-volatile recycling.

While data resolution limitations and the need for further verification prevent definitive conclusions, geomorphological features remain a valuable surface marker for subsurface processes. The underlying processes remain universally applicable despite the scaling difference between Earth and Pluto. The findings of our research will play a pivotal role in addressing first-order questions relevant not only to Pluto but also to other icy worlds. Such questions could investigate the relationship between pit characteristics and properties of fluid sources or plumbing systems to better constrain the presence, location, and extent of potential volatile reservoirs in Pluto's subsurface. These pits could have important implications for Pluto's broader geophysical and atmospheric evolution.

## Conflict of Interest

The authors declare no conflicts of interest relevant to this study.



21699100, 2026, 3, Downloaded from https://agupubs.onlinelibrary.wiley.com/doi/10.1029/2025JE009252 by Nasa Goddard, Wiley Online Library on [02/03/2026]. See the Terms and Conditions (https://onlinelibrary.wiley.com/terms-and-conditions) on Wiley Online Library for rules of use; OA articles are governed by the applicable Creative Commons License

## Data Availability Statement

The global mosaic and DEM of Pluto (Schenk et al., 2018) used in this work are publicly available in JMARS (Christensen et al., 2009). They are also available from the Planetary Data Systems Small Bodies Node https://pds-smallbodies.astro.umd.edu/data_sb/missions/newhorizons/index.shtml in the "New Horizons Pluto Encounter Geology and Geophysical Maps" directory, and can be downloaded at the following links: (a) Global mosaic: https://astrogeology.usgs.gov/search/map/pluto_new_horizons_lorri_mvic_global_mosaic_300m and (b) Global DEM: https://astrogeology.usgs.gov/search/map/pluto_new_horizons_lorri_mvic_global_dem_300m. The band depth maps are available from the Planetary Data Systems Small Bodies at the following link https://pds-smallbodies.astro.umd.edu/holdings/pds4-nh_derived-v4.0/plutosystem_composition/absorp/. The data set of the morphological characteristics and measurements for pits analyzed in this study is publicly available in the Zenodo repository (Manogaran, 2025). *Software availability statement*: This work used Java Mission-planning and Analysis for Remote Sensing (JMARS v.5.3.0), Tableau Desktop (Professional Edition v.2024.2.2), QGIS (v.3.40.5-Bratislava), and Visual Studio Code (v.1.96.4) for data visualization and analysis. JMARS is a free online geographic information system from Arizona State University, available at https://jmars.asu.edu/ (Christensen et al., 2009).

**Acknowledgments**

R. Manogaran, G. Poh, and C. Ahrens are supported through a cooperative agreement with Center for Research and Exploration in Space Sciences and Technology II (CRESST II) between NASA Goddard Space Flight Center, Catholic University of America, and University of Maryland College Park; the material is based upon work supported by NASA under award number 80GSFC24M0006. K.E.M. acknowledges support from NASA ROSES DDAP Grant 80NSSC25K0001. We thank the two anonymous reviewers and the Associate Editor for their constructive reviews, which greatly improved this manuscript. We also thank Jay Friedlander for assistance with preparing the digital version of Figure 7 based on the authors' original sketch.

## References

Andresen, K. J., Huuse, M., & Clausen, O. (2008). Morphology and distribution of Oligocene and Miocene pockmarks in the Danish North Sea–implications for bottom current activity and fluid migration. *Basin Research*, *20*(3), 445–466. https://doi.org/10.1111/j.1365-2117.2008.00362.x

Audsley, A., Bradwell, T., Howe, J. A., & Baxter, J. M. (2019). Distribution and classification of pockmarks on the seabed around western Scotland. *Journal of Maps*, *15*(2), 807–817. https://doi.org/10.1080/17445647.2019.1676320

Batchelor, C. L., Frinault, B. A., Christie, F. D., Montelli, A., & Dowdeswell, J. A. (2022). The morphology of pockmarks on the north-east Antarctic Peninsula continental shelf. *Antarctic Science*, *34*(4), 313–324. https://doi.org/10.1017/s0954102022000177

Binzel, R. P., Earle, A. M., Buie, M. W., Young, L. A., Stern, S. A., Olkin, C. B., et al. (2017). Climate zones on Pluto and Charon. *Icarus*, *287*, 30–36. https://doi.org/10.1016/j.icarus.2016.07.023

Boström, M., Esteso, V., Fiedler, J., Brevik, I., Buhmann, S. Y., Persson, C., et al. (2021). Self-preserving ice layers on CO2 clathrate particles: Implications for Enceladus, Pluto, and similar ocean worlds. *Astronomy and Astrophysics*, *650*, A54.

Carnahan, E., Vance, S. D., Hesse, M. A., Journaux, B., & Sotin, C. (2022). Dynamics of mixed clathrate-ice shells on ocean worlds. *Geophysical Research Letters*, *49*(8), e2021GL097602. https://doi.org/10.1029/2021gl097602

Cathles, L., Su, Z., & Chen, D. (2010). The physics of gas chimney and pockmark formation, with implications for assessment of seafloor hazards and gas sequestration. *Marine and Petroleum Geology*, *27*(1), 82–91. https://doi.org/10.1016/j.marpetgeo.2009.09.010

Cawood, A. J., Ferrill, D. A., & Smart, K. J. (2024). Failure modes and fault morphology. *Lithosphere*. https://doi.org/10.2113/2024/lithosphere_2024_162

Ceramicola, S., Dupré, S., Somoza, L., & Woodside, J. (2018). Cold seep systems. *Submarine Geomorphology*, 367–387.

Christensen, P., Engle, E., Anwar, S., Dickenshied, S., Noss, D., Gorelick, N., & Weiss-Malik, M. (2009). JMARS-a planetary GIS [Software]. *AGU Fall Meeting*. http://ui.adsabs.harvard.edu/abs/2009AGUFMIN22A..06C/abstract

Chuvilin, E., Bukhanov, B., Davletshina, D., Grebenkin, S., & Istomin, V. (2018). Dissociation and self-preservation of gas hydrates in permafrost. *Geosciences*, *8*(12), 431. https://doi.org/10.3390/geosciences8120431

Chuvilin, E., Ekimova, V., Davletshina, D., Sokolova, N., & Bukhanov, B. (2020). Evidence of gas emissions from permafrost in the Russian Arctic. *Geosciences*, *10*(10), 383. https://doi.org/10.3390/geosciences10100383

Courville, S. W., Castillo-Rogez, J. C., Daswani, M. M., Gloesener, E., Choukroun, M., & O'Rourke, J. G. (2023). Timing and abundance of clathrate Formation control Ocean evolution in outer solar system bodies: Challenges of maintaining a thick ocean within Pluto. *The Planetary Science Journal*, *4*(9), 179. https://doi.org/10.3847/psj/acf377

Cronin, B. T., & Jubilee Team, T. G. L. (2022). Giant pockmark-initiated deep-water slope channel complexes. *AAPG Bulletin*, *106*(4), 829–868. https://doi.org/10.1306/11042118179

Cruikshank, D. P., Dalle Ore, C. M., Scipioni, F., Beyer, R. A., White, O. L., Moore, J. M., et al. (2021). Cryovolcanic flooding in viking terra on Pluto. *Icarus*, *356*, 113786. https://doi.org/10.1016/j.icarus.2020.113786

Cruikshank, D. P., Umurhan, O. M., Beyer, R. A., Schmitt, B., Keane, J. T., Runyon, K. D., et al. (2019). Recent cryovolcanism in virgil fossae on Pluto. *Icarus*, *330*, 155–168. https://doi.org/10.1016/j.icarus.2019.04.023

Dalle Ore, C., Cruikshank, D., Protopapa, S., Scipioni, F., McKinnon, W., Cook, J., et al. (2019). Detection of ammonia on Pluto's surface in a region of geologically recent tectonism. *Science Advances*, *5*(5), eaav5731. https://doi.org/10.1126/sciadv.aav5731

Dandapath, S., Chakraborty, B., Karisiddaiah, S. M., Menezes, A., Ranade, G., Fernandes, W., et al. (2010). Morphology of pockmarks along the western continental margin of India: Employing multibeam bathymetry and backscatter data. *Marine and Petroleum Geology*, *27*(10), 2107–2117. https://doi.org/10.1016/j.marpetgeo.2010.09.005

Earle, A. M., Binzel, R. P., Young, L. A., Stern, S., Ennico, K., Grundy, W., et al. (2017). Long-term surface temperature modeling of Pluto. *Icarus*, *287*, 37–46. https://doi.org/10.1016/j.icarus.2016.09.036

Emran, A., Dalle Ore, C., Ahrens, C., Khan, M., Chevrier, V., & Cruikshank, D. P. (2023). Pluto's surface mapping using unsupervised learning from near-infrared observations of LEISA/Ralph. *The Planetary Science Journal*, *4*(1), 15. https://doi.org/10.3847/psj/acb0cc

Enoh, M. A., Okeke, F. I., & Okeke, U. C. (2021). Automatic lineaments mapping and extraction in relationship to natural hydrocarbon seepage in Ugwueme, South-Eastern Nigeria. *Geodesy and Cartography*, *47*(1), 34–44. https://doi.org/10.3846/gac.2021.12099

Etiope, G., Ehlmann, B. L., & Schoell, M. (2013). Low temperature production and exhalation of methane from serpentinized rocks on Earth: A potential analog for methane production on Mars. *Icarus*, *224*(2), 276–285. https://doi.org/10.1016/j.icarus.2012.05.009

Forwick, M., Baeten, N. J., & Vorren, T. O. (2009). Pockmarks in Spitsbergen fjords. *Norwegian Journal of Geology/Norsk Geologisk Forening*, *89*.



21699100, 2026, 3, Downloaded from https://agupubs.onlinelibrary.wiley.com/doi/10.1029/2025JE009252 by Nasa Goddard, Wiley Online Library on [02/03/2026]. See the Terms and Conditions (https://onlinelibrary.wiley.com/terms-and-conditions) on Wiley Online Library for rules of use; OA articles are governed by the applicable Creative Commons License

Frederick, J., & Buffett, B. (2014). Taliks in relict submarine permafrost and methane hydrate deposits: Pathways for gas escape under present and future conditions. *Journal of Geophysical Research: Earth Surface*, *119*(2), 106–122. https://doi.org/10.1002/2013jf002987
Gafeira, J., Dolan, M. F., & Monteys, X. (2018). Geomorphometric characterization of pockmarks by using a GIS-based semi-automated toolbox. *Geosciences*, *8*(5), 154. https://doi.org/10.3390/geosciences8050154
Grundy, W., Binzel, R., Buratti, B., Cook, J., Cruikshank, D., Dalle Ore, C., et al. (2016). Surface compositions across Pluto and Charon. *Science*, *351*(6279), aad9189. https://doi.org/10.1126/science.aad9189
Grundy, W., Wong, I., Glein, C., Protopapa, S., Holler, B., Cook, J., et al. (2024). Measurement of D/H and 13C/12C ratios in methane ice on Eris and Makemake: Evidence for internal activity. *Icarus*, *411*, 115923. https://doi.org/10.1016/j.icarus.2023.115923
Gupta, S., & Micallef, A. (2023). Modelling the influence of erosive fluidization on the morphology of fluid flow and escape structures. *Mathematical Geosciences*, *55*(8), 1101–1123. https://doi.org/10.1007/s11004-023-10071-z
Gupta, S., Schmidt, C., Böttner, C., Rüpke, L., & Hartz, E. H. (2022). Spontaneously exsolved free gas during major storms as an ephemeral gas source for pockmark formation. *Geochemistry, Geophysics, Geosystems*, *23*(8), e2021GC010289. https://doi.org/10.1029/2021gc010289
Hand, K., Sotin, C., Hayes, A., & Coustenis, A. (2020). On the habitability and future exploration of ocean worlds. *Space Science Reviews*, *216*(5), 1–24. https://doi.org/10.1007/s11214-020-00713-7
Hedgepeth, J. E., Neish, C. D., & Bray, V. J. (2023). Impact Crater morphometry on Pluto: Implications for surface composition and evolution. *The Planetary Science Journal*, *4*(10), 190. https://doi.org/10.3847/psj/acf934
Hovland, M. (2012). The Geomorphology and nature of seabed seepage processes. In P. Blondel (Ed.), *Bathymetry and its applications* (pp. 79–104). IntechOpen: Rjeka.
Hovland, M., Gardner, J. V., & Judd, A. (2002). The significance of pockmarks to understanding fluid flow processes and geohazards. *Geofluids*, *2*(2), 127–136. https://doi.org/10.1046/j.1468-8123.2002.00028.x
Howard, A. D., Moore, J. M., Umurhan, O. M., White, O. L., Singer, K. N., & Schenk, P. M. (2023). Are the surface textures of Pluto's Wright Mons and its surroundings exogenic? *Icarus*, *405*, 115719. https://doi.org/10.1016/j.icarus.2023.115719
Howard, A. D., Moore, J. M., White, O. L., Umurhan, O. M., Schenk, P. M., Grundy, W. M., et al. (2017). Pluto: Pits and mantles on uplands north and east of Sputnik Planitia. *Icarus*, *293*, 218–230. https://doi.org/10.1016/j.icarus.2017.02.027
Kamata, S., Nimmo, F., Sekine, Y., Kuramoto, K., Noguchi, N., Kimura, J., & Tani, A. (2019). Pluto's ocean is capped and insulated by gas hydrates. *Nature Geoscience*, *12*(6), 407–410. https://doi.org/10.1038/s41561-019-0369-8
Keane, J. T., Matsuyama, I., Kamata, S., & Steckloff, J. K. (2016). Reorientation and faulting of Pluto due to volatile loading within Sputnik Planitia. *Nature*, *540*(7631), 90–93. https://doi.org/10.1038/nature20120
Kling, C. L., Byrne, P. K., Atkins, R. M., & Wegmann, K. W. (2021). Tectonic deformation and volatile loss in the formation of Noctis Labyrinthus, Mars. *Journal of Geophysical Research: Planets*, *126*(11), e2020JE006555. https://doi.org/10.1029/2020je006555
Kluesner, J. W., Silver, E. A., Bangs, N. L., McIntosh, K. D., Gibson, J., Orange, D., et al. (2013). High density of structurally controlled, shallow to deep water fluid seep indicators imaged offshore Costa Rica. *Geochemistry, Geophysics, Geosystems*, *14*(3), 519–539. https://doi.org/10.1002/ggge.20058
Kvenvolden, K. A. (1993). Gas hydrates—Geological perspective and global change. *Reviews of Geophysics*, *31*(2), 173–187. https://doi.org/10.1029/93rg00268
Lellouch, E., Stansberry, J., Emery, J., Grundy, W., & Cruikshank, D. P. (2011). Thermal properties of Pluto's and Charon's surfaces from Spitzer observations. *Icarus*, *214*(2), 701–716. https://doi.org/10.1016/j.icarus.2011.05.035
Loncke, L., Mascle, J., & Parties, F. S. (2004). Mud volcanoes, gas chimneys, pockmarks and mounds in the Nile deep-sea fan (Eastern Mediterranean): Geophysical evidences. *Marine and Petroleum Geology*, *21*(6), 669–689. https://doi.org/10.1016/j.marpetgeo.2004.02.004
Lopes, R. M., Kirk, R. L., Mitchell, K. L., LeGall, A., Barnes, J. W., Hayes, A., et al. (2013). Cryovolcanism on Titan: New results from Cassini RADAR and VIMS. *Journal of Geophysical Research: Planets*, *118*(3), 416–435. https://doi.org/10.1002/jgre.20062
Madrussani, G., Rossi, G., & Camerlenghi, A. (2010). Gas hydrates, free gas distribution and fault pattern on the west Svalbard continental margin. *Geophysical Journal International*, *180*(2), 666–684. https://doi.org/10.1111/j.1365-246x.2009.04425.x
Manogaran, R. (2025). Geomorphological evidence of fluid seepage in pit complex Formation [Dataset]. *Pioneer Terra, Pluto*. https://doi.org/10.5281/zenodo.17835856
Martin, C. R., & Binzel, R. P. (2021). Ammonia-water freezing as a mechanism for recent cryovolcanism on Pluto. *Icarus*, *356*, 113763. https://doi.org/10.1016/j.icarus.2020.113763
Martin, E. S., Kattenhorn, S. A., Collins, G. C., Michaud, R. L., Pappalardo, R. T., & Wyrick, D. Y. (2017). Pit chains on Enceladus signal the recent tectonic dissection of the ancient cratered terrains. *Icarus*, *294*, 209–217. https://doi.org/10.1016/j.icarus.2017.03.014
McGovern, P. J., White, O. L., & Schenk, P. M. (2021). Tectonism and enhanced cryovolcanic potential around a loaded Sputnik Planitia basin, Pluto. *Journal of Geophysical Research: Planets*, *126*(12), e2021JE006964. https://doi.org/10.1029/2021je006964
McKinnon, W. B., Glein, C. R., Bertrand, T., & Rhoden, A. R. (2020). Formation, composition, and history of the Pluto System: A post-new-horizons synthesis. *arXiv preprint arXiv:2011.14030*.
Moore, J. M., & Howard, A. D. (2021). The landscapes of Pluto as witness to climate evolution. *The Pluto System After New Horizons*, *105*.
Moore, J. M., Howard, A. D., Umurhan, O. M., White, O. L., Schenk, P. M., Beyer, R. A., et al. (2017). Sublimation as a landform-shaping process on Pluto. *Icarus*, *287*, 320–333. https://doi.org/10.1016/j.icarus.2016.08.025
Moore, J. M., McKinnon, W. B., Spencer, J. R., Howard, A. D., Schenk, P. M., Beyer, R. A., et al. (2016). The geology of Pluto and charon through the eyes of new Horizons. *Science*, *351*(6279), 1284–1293. https://doi.org/10.1126/science.aad7055
Oehler, D. Z., & Etiope, G. (2017). Methane seepage on Mars: Where to look and why. *Astrobiology*, *17*(12), 1233–1264. https://doi.org/10.1089/ast.2017.1657
Omeru, T., Ayerume, D., Bankole, S., Ogbe, O. B., Byami, J. A., Obafemi, S., et al. (2021). Geomorphometric analysis of seabed pockmarks, offshore western Niger Delta: A case study of the freeman field. *Interpretation*, *9*(2), T569–T584. https://doi.org/10.1190/int-2020-0154.1
Pei, Y., Paton, D. A., Knipe, R. J., & Wu, K. (2015). A review of fault sealing behaviour and its evaluation in siliciclastic rocks. *Earth-Science Reviews*, *150*, 121–138. https://doi.org/10.1016/j.earscirev.2015.07.011
Pilcher, R., & Argent, J. (2007). Mega-pockmarks and linear pockmark trains on the West African continental margin. *Marine Geology*, *244*(1–4), 15–32. https://doi.org/10.1016/j.margeo.2007.05.002
QGIS Development Team. (2022). QGIS geographic information system [Software]. *Open Source Geospatial Foundation Project*. Retrieved from https://qgis.org
Riboulot, V., Sultan, N., Imbert, P., & Ker, S. (2016). Initiation of gas-hydrate pockmark in deep-water Nigeria: Geo-mechanical analysis and modelling. *Earth and Planetary Science Letters*, *434*, 252–263. https://doi.org/10.1016/j.epsl.2015.11.047
Robbins, S. J., & Dones, L. (2023). Impact crater databases for Pluto and charon, version 2. *The Planetary Science Journal*, *4*(12), 233. https://doi.org/10.3847/psj/acf7be



21699100, 2026, 3, Downloaded from https://agupubs.onlinelibrary.wiley.com/doi/10.1029/2025JE009252 by Nasa Goddard, Wiley Online Library on [02/03/2026]. See the Terms and Conditions (https://onlinelibrary.wiley.com/terms-and-conditions) on Wiley Online Library for rules of use; OA articles are governed by the applicable Creative Commons License

Rodríguez, J. A. P., Sasaki, S., Dohm, J. M., Tanaka, K. L., Strom, B., Kargel, J., et al. (2005). Control of impact crater fracture systems on subsurface hydrology, ground subsidence, and collapse, Mars. *Journal of Geophysical Research*, *110*(E6).
Schenk, P. M., Beyer, R. A., McKinnon, W. B., Moore, J. M., Spencer, J. R., White, O. L., et al. (2018). Basins, fractures and volcanoes: Global cartography and topography of Pluto from New Horizons [Dataset]. *Icarus*, *314*, 400–433. https://doi.org/10.1016/j.icarus.2018.06.008
Schmitt, B., Philippe, S., Grundy, W., Reuter, D., Côte, R., Quirico, E., et al. (2017). Physical state and distribution of materials at the surface of Pluto from New Horizons LEISA imaging spectrometer. *Icarus*, *287*, 229–260. https://doi.org/10.1016/j.icarus.2016.12.025
Singer, K. N., Greenstreet, S., Schenk, P., Robbins, S., & Bray, V. (2021). Impact craters on Pluto and Charon and terrain age estimates. *The Pluto System After New Horizons*, 121–145.
Singer, K. N., McKinnon, W. B., & Schenk, P. M. (2021). Pits, uplifts and small chaos features on Europa: Morphologic and morphometric evidence for intrusive upwelling and lower limits to ice shell thickness. *Icarus*, *364*, 114465. https://doi.org/10.1016/j.icarus.2021.114465
Singer, K. N., White, O. L., Schmitt, B., Rader, E. L., Protopapa, S., Grundy, W. M., et al. (2022). Large-scale cryovolcanic resurfacing on Pluto. *Nature Communications*, *13*(1), 1542. https://doi.org/10.1038/s41467-022-29056-3
Stern, S. A., Grundy, W. M., McKinnon, W. B., Weaver, H. A., & Young, L. A. (2018). The Pluto system after new horizons. *Annual Review of Astronomy and Astrophysics*, *56*(1), 357–392. https://doi.org/10.1146/annurev-astro-081817-051935
Stern, S. A., White, O., McGovern, P., Keane, J., Conrad, J., Bierson, C., et al. (2021). Pluto's far side. *Icarus*, *356*, 113805.
Strozyk, F., Reuning, L., Back, S., & Kukla, P. (2018). Giant pockmark formation from Cretaceous hydrocarbon expulsion in the western Lower Saxony Basin, the Netherlands. *Geological Society, London, Special Publications*, *469*(1), 519–536. https://doi.org/10.1144/sp469.6
Sun, Q., Wu, S., Hovland, M., Luo, P., Lu, Y., & Qu, T. (2011). The morphologies and genesis of mega-pockmarks near the Xisha uplift, South China Sea. *Marine and Petroleum Geology*, *28*(6), 1146–1156. https://doi.org/10.1016/j.marpetgeo.2011.03.003
Szpak, M. T., Monteys, X., O'Reilly, S. S., Lilley, M. K., Scott, G. A., Hart, K. M., et al. (2015). Occurrence, characteristics and formation mechanisms of methane generated micro-pockmarks in Dunmanus Bay, Ireland. *Continental Shelf Research*, *103*, 45–59. https://doi.org/10.1016/j.csr.2015.04.023
Tableau Desktop (Professional Edition 2024.2.2). (2024). Tableau desktop (professional edition 2024.2.2) [Software]. Retrieved from https://www.tableau.com/products/desktop
Talukder, A. R. (2012). Review of submarine cold seep plumbing systems: Leakage to seepage and venting. *Terra Nova*, *24*(4), 255–272. https://doi.org/10.1111/j.1365-3121.2012.01066.x
Tobie, G., Lunine, J. I., & Sotin, C. (2006). Episodic outgassing as the origin of atmospheric methane on Titan. *Nature*, *440*(7080), 61–64. https://doi.org/10.1038/nature04497
Visual Studio Code. (2024). Visual studio code [Software]. Retrieved from https://code.visualstudio.com/download
Webb, K. E., Hammer, Ø., Lepland, A., & Gray, J. S. (2009). Pockmarks in the inner Oslofjord, Norway. *Geo-Marine Letters*, *29*(2), 111–124. https://doi.org/10.1007/s00367-008-0127-1
Weinberger, J. L., & Brown, K. M. (2006). Fracture networks and hydrate distribution at Hydrate ridge, Oregon. *Earth and Planetary Science Letters*, *245*(1–2), 123–136. https://doi.org/10.1016/j.epsl.2006.03.012
White, O., Moore, J., Howard, A., Schenk, P., Singer, K., Williams, D., & Lopes, R. (2021). The geology of Pluto. *The Pluto System After New Horizons*, 55–87.
Wu, Z., Zhao, D., Zhou, J., Liu, Z., Wang, M., Shang, J., et al. (2023). Formation mechanism of deep-sea giant pockmarks: A case study of the reed basin in the South China Sea. *Geomorphology*, *433*, 108726. https://doi.org/10.1016/j.geomorph.2023.108726
Wyrick, D., & Buczkowski, D. (2022). Pit crater chains across the solar system: Evidence for subterranean tectonic caves, porosity and permeability pathways on planetary bodies. *Journal of Geophysical Research: Planets*, *127*(12), e2022JE007281. https://doi.org/10.1029/2022je007281
Wyrick, D., Ferrill, D. A., Morris, A. P., Colton, S. L., & Sims, D. W. (2004). Distribution, morphology, and origins of Martian pit crater chains. *Journal of Geophysical Research*, *109*(E6). https://doi.org/10.1029/2004je002240
Zhang, K., Guan, Y., Song, H., Fan, W., Li, H., Kuang, Y., & Geng, M. (2020). A preliminary study on morphology and genesis of giant and mega pockmarks near Andu Seamount, Nansha region (South China Sea). *Marine Geophysical Research*, *41*, 1–12. https://doi.org/10.1007/s11001-020-09404-y
Zhang, K., Song, H., Chen, J., Geng, M., & Liu, B. (2023). Gas seepage detection and gas migration mechanisms. In *South China sea seeps* (pp. 35–53). Singapore: Springer Nature Singapore.
Zhang, Q., Alves, T. M., & Martins-Ferreira, M. A. C. (2025). Buried pockmarks associated with listric faults of salt minibasins (Espírito Santo, SE Brazil): Evidence for local hydrocarbon escape since the miocene. *Basin Research*, *37*(1), e70015. https://doi.org/10.1111/bre.70015
Zhang, Z., Deng, X., Yao, H., Yu, M., Wang, H., He, G., et al. (2021). A preliminary study on geomorphological characteristics and genetic mechanism of pockmarks in the Makran accretionary prism, northern Arabian Sea. *Geo-Marine Letters*, *41*(3), 27. https://doi.org/10.1007/s00367-021-00704-9



21699100, 2026, 3, Downloaded from https://agupubs.onlinelibrary.wiley.com/doi/10.1029/2025JE009252 by Nasa Goddard, Wiley Online Library on [02/03/2026]. See the Terms and Conditions (https://onlinelibrary.wiley.com/terms-and-conditions) on Wiley Online Library for rules of use; OA articles are governed by the applicable Creative Commons License